

1 A 1998-2013 climatology of Kyushu, Japan:

2 Seasonal variations of stability and rainfall

3 Alexandros P. Poulidis<sup>1</sup> and Tetsuya Takemi<sup>1</sup>

4

5 **Short title:** A 1998–2013 sounding and rainfall climatology of Kyushu, Japan

6 **Keywords:** rawinsonde, rainfall, climatology, rainy season, Japan, Kyushu

7 **Corresponding author:** A. P. Poulidis, Disaster Prevention Research Institute,

8 Kyoto University, Gokasho, Uji, 611-0011, Japan (a.poulidis@storm.dpri.kyoto-u.ac.jp)

9 **Affiliations:** <sup>1</sup>Disaster Prevention Research Institute, Kyoto University

## Abstract

The seasonal variation of the atmospheric structure, vertical shear, stability and rainfall distribution over the island of Kyushu, southern Japan, is studied using 16 years of observational data, from 1998 to 2013. Over 20000 twice-daily rawinsonde observations from the cities of Kagoshima (southern Kyushu) and Fukuoka (northern Kyushu) are utilised along with daily precipitation data from 120 Japan Meteorological Agency stations located across the island. Understanding the local atmospheric circulation and climatological behaviour of the island is important both locally due to the island's large population and regionally, due to its position in relation to the tracks of typhoons generated annually over the Pacific ocean and make landfall here, the rainy season associated with the Asian monsoon, and the large number of active volcanoes located on or near the island, emitting volcanic gases and ash on a daily basis.

Using a categorisation based on convective available potential energy and precipitable water, three sounding categories are distinguished, described using the origins of the air masses involved, as seen from trajectory modelling: Continental (Dry), Oceanic (Moist/Unstable), and Mixed (Moist/Stable). Mean soundings for each category are examined, along with information on their annual and seasonal variability. Each sounding category is linked with a rainfall response: low amounts of rainfall, heavy convective rainfall, and heavy, non-convective rainfall respectively. Despite the large difference in the potential for heavy rainfall rates, average daily rainfall rate is similar for the two moist categories, but peak rainfall rates for convective rainfall are twice as large as those for non-convective. Despite the simplicity of the criteria, the

35 three sounding categories are statistically robust and exhibit a relatively small  
36 amount of variability. The monthly combination of the sounding categories  
37 is shown to be a deciding factor in the seasonal variation of the atmospheric  
38 circulation, weather, and precipitation over the island.

# 1 Introduction

Seasonal variability is a well known characteristic of Japanese climate, ingrained in Japanese culture with innumerable mentions of the “four seasons” (shiki) in Japanese literature and arts (Ackermann, 1997). This seasonality stems from the combination of several stationary weather systems and fronts (Uvo *et al.*, 2001). In the south of Japan, during the winter season (December, January, February or DJF in figures) air flow towards Japan is mainly controlled by the stationary Siberian High and Aleutian Low systems leading to low amounts of precipitation (Kazaoka and Kida, 2006). In spring (MAM) the weather is mainly forced by transient mid-latitude synoptic cyclones, while in late spring and early to mid-summer (JJA) the weather is mainly characterised by the East Asian rainy season. This is caused by the Baiu/Meiyu stationary front (Wang and Ho, 2002): Dry continental air masses are mixed with moist air forced from the Pacific brought by the Pacific High resulting to large amounts of rainfall between May and July. Towards the end of the summer and throughout the majority of autumn (SON) the weather is largely characterised by the Summer Monsoon, typhoons, and other tropical low pressure systems (Gray, 1968). Although these are typical elements of the Japanese climate in general, different parts of Japan are affected to differing degrees as the Japanese islands stretch between longitudes of 24°–45° N.

The island of Kyushu is the southernmost of the four main islands (approximately 131° E and 33° N; Fig. 1a). It has the second highest population density (332.38 km<sup>-2</sup>) after the main island of Honshu. The topography of the island is complex, characterised by the numerous peaks of the Kyushu mountains, the highest peak

62 being Mount Nakadake of the Kuju mountains at 1791 m. Kyushu is also home to a  
63 number of active volcanoes, such as Mounts Unzen, Sakurajima, Aso and Kirishima.

64 Most Japanese islands are prone to natural hazards with earthquakes, volcanic  
65 eruptions, floods, and landslides amongst others. The location of Kyushu towards  
66 the south-western end of the island chain exacerbates rainfall-related hazards; the  
67 island comes under the influence of different continental and tropical/subtropical  
68 airmasses and the Asian monsoon resulting in large amounts of rainfall during the  
69 Baiu season (Uvo *et al.*, 2001). After the Baiu season, a large number of typhoons  
70 makes landfall at Kyushu (Goh and Chan, 2012; Grossman *et al.*, 2014). Owing  
71 to the south-north direction alignment of the Kyushu mountains across the centre  
72 of the island, the eastern (windward) part of Kyushu is more heavily affected by  
73 rainfall. Intense rainfall can in itself be a primary hazard causing flooding, but it can  
74 also trigger secondary hazards such as landslides (Kato, 2005; Unuma and Takemi,  
75 2016) and volcanic mudflows/lahars (Miyabuchi *et al.*, 2004). Finally, rainfall has  
76 been implicated for initiating volcanic eruptions for certain types of volcanoes such  
77 as Mount Unzen (Yamasato *et al.*, 1998), a phenomenon also seen in a number of  
78 volcanoes outside of Japan such as Mount St. Helens, USA (Mastin, 1994), and  
79 Soufrière Hills, Montserrat (Matthews *et al.*, 2002; Carn *et al.*, 2004; Barclay *et al.*,  
80 2006).

81 The seasonal variation of wind, rainfall, and stability also have an immediate  
82 impact on the dispersal of the volcanic emissions from the volcanoes on the island, as  
83 they are the primary deciding factors in the transport, deposition, and remobilisation  
84 of volcanic ash (Bonadonna *et al.*, 2012; Wilson *et al.*, 2012). Many of the island's

85 volcanoes erupt frequently, while in the case of the Sakurajima volcano ash and  
86 volcanic gasses are released almost continuously by eruptions or as passive emissions  
87 (Iguchi, 2016). Long-term exposure to these volcanic emissions is known to impact  
88 the surrounding communities (Hillman *et al.*, 2012). Studying the climatology of  
89 the island can thus help gain a deeper understanding of the seasonality of these  
90 emissions and help in the long-term hazard management.

91 Despite the fact that both the Baiu and the typhoon season receive a large  
92 amount of attention, research has tended to focus on specific phenomena (for ex-  
93 ample Yoshizaki *et al.*, 2000; Uvo *et al.*, 2001; Kato, 2005; Nishiyama *et al.*, 2007;  
94 Takemi, 2007a,b; Goh and Chan, 2012; Grossman *et al.*, 2014; Iwasaki, 2014; Takemi,  
95 2014; Unuma and Takemi, 2016). A previous climatological study by Chuda and  
96 Niino (2005) focused on the seasonal evolution of stability parameters and precip-  
97 itable water content in different parts of Japan. The study concluded that on average  
98  $\text{PW}_{\text{max}}$  exhibits a smooth, monotonic behaviour, while high value of  $\text{CAPE}_{\text{max}}$  are mainly  
99 constrained between July and September. It was also noted that higher values of  
100 CAPE are observed in the south than the north; however detailed analysis over  
101 specific parts of Japan was deemed necessary in order to understand the effect of  
102 large-scale systems on the parameters. The study did not cover the vertical struc-  
103 ture of the atmosphere in detail: this is the aim of this paper and to our knowledge,  
104 the first of this kind in the area. It is our hope that these characteristic profiles will  
105 be used as benchmarks for climatological and modelling studies of the area, simi-  
106 lar to work carried out for midlatitude convective storms over the continental US  
107 (Bluestein and Jain, 1985) and the rainy season in the Caribbean (Dunion, 2011),

108 and as the atmospheric context for further research on natural hazards focusing on  
109 the Baiu, typhoons, volcanic activity, or landslides.

110 Due to the focus of this work on the broad seasonal behaviours and categorisa-  
111 tions of the climate, local circulation, and resulting weather, the finer details of each  
112 sounding category will have to be ignored for the time being; the results presented  
113 here concern the average response to specific mesoscale conditions. In reality due  
114 to the position and the complexity of the topography a large number of well-known  
115 but finer-scale phenomena occur, for example heavy convective rainfall over weaker  
116 non-convective rainfall (Akiyama, 1978; Houze Jr, 1997) and the Koshikijima and  
117 Nagasaki rainbands (Ninomiya and Yamazaki, 1979; Kato, 2005). Although these  
118 are not studied in detail they offer a possible future extension using the main frame-  
119 work presented here.

120 The paper is organised as follows. Section 2 contains a short description of the  
121 observational data and the numerical modelling carried out. The categorisation  
122 criteria and resulting trajectories per category are presented in Section 3. Different  
123 sounding types (both seasonal and per sounding category) and the corresponding  
124 rainfall patterns are presented and discussed in Sections 4 and 5 respectively. The  
125 main conclusions of the study are summarised in Section 6.

## 126 2 Data and Methodology

### 127 2.1 Observations

128 The study period is from the 1st of January 1998 to the 31st of December 2013.  
129 Kyushu is covered by more than 160 meteorological stations maintained by the  
130 Japan Meteorological Agency (JMA), creating a relatively high-resolution observa-  
131 tion network, approximately 17 km spatial resolution (Fig. 1). Rawinsonde stations  
132 are located at Kagoshima [southern Kyushu; World Meteorological Organisation  
133 (WMO) code: 47827, 31.55°N/130.55°E] and Fukuoka (Northern Kyushu; WMO  
134 code: 47807, 33.58°N/130.38°E), with rawinsondes launched twice daily (at 0000 and  
135 1200 UTC). Sounding data can be accessed from the University of Wyoming archive  
136 website ([weather.uwyo.edu/upperair/sounding.html](http://weather.uwyo.edu/upperair/sounding.html)). Rainfall data are measured  
137 in 10-min intervals by the Japanese nation-wide meteorological network (Auto-  
138 mated Meteorological Data Acquisition System; AMeDAS). Archived data are freely  
139 available in various formats (hourly, daily, monthly averages and daily maximums  
140 of 10-min and 1-h rainfall intensity) and can be accessed from the JMA website  
141 ([www.data.jma.go.jp/gmd/risk/obsdl/](http://www.data.jma.go.jp/gmd/risk/obsdl/)). Here we use the daily average [referred  
142 to as *daily rainfall* ( $R_d$ ) in the remainder of the paper] and daily 10-min rainfall  
143 intensity maximum (*peak rainfall intensity*;  $R_{10}$ ).

144 Soundings that did not contain non-humidity-based parameter data at all ra-  
145 diosonde observation mandatory levels (1000, 925, 850, 700, 500, 400, 300, 250,  
146 200, 150, 100, and 50 hPa) or humidity-based parameter data up to 400 hPa were  
147 rejected. As in Dunion (2011), in addition to data presented at radiosonde ob-



148 servation mandatory levels, a linearly interpolated value is also shown at 600 hPa  
149 due to the relatively large gap between the 700 and 500 hPa levels (approximately  
150 2700 m difference in height). Using other interpolation methods (cubic or spline)  
151 showed little difference in the results. Estimates for water vapour mixing ratio above  
152 400 hPa are provided using the European Centre for Medium-Range Weather Fore-  
153 casts (ECMWF) Re-Analysis data set (ERA-Interim; Dee *et al.*, 2011). The ERA-  
154 Interim mixing ratio values were adjusted above 400 hPa to avoid discontinuity in  
155 the data. Other humidity-based parameters were calculated using the ERA-Interim  
156 mixing ratio data. Statistical analysis for wind speed data was carried out using  
157 the vector wind speed (value presented in the sounding data), while for wind di-  
158 rection, the wind vector was analysed in  $U$  and  $V$  components and the final wind  
159 direction statistics were calculated as the results of the analysis of the individual  
160 components.

161 Although there are 169 rainfall stations covering Kyushu and the surrounding  
162 islands, a number of them have intermittent data. Data from stations covering less  
163 than 90% of the study period can compromise the statistical analysis results (Lau  
164 and Sheu, 1988), and thus, the stations were split into two categories, “safe” (120  
165 stations) and “compromised” (49). Among the “safe” stations, average  
166 data availability is 99.9% of the study period, with a minimum of 98%. Similar  
167 results were noted by Uvo *et al.* (2001). Amongst the “compromised” stations,  
168 results vary with stations providing coverage for as little as 1% and as much as  
169 88% of the study period. When results from all stations are shown there will be a  
170 clear distinction between the stations categories. In our study statistical analysis is

171 carried out using the “safe” stations, but inclusion of all stations did not affect the  
172 results drastically. Sounding data were converted from UTC to Japanese Standard  
173 Time (JST; JST=UTC+9). All references to dates made here use JST. Results  
174 presented were tested for statistical significance using a two-tailed Student’s  $t$  test  
175 at a 95–99.9 confidence level. The statistical checks carried out are described in  
176 detail in each section.

## 177 **2.2 The HYSPLIT model**

178 The Hybrid Single-Particle Lagrangian Integrated Trajectory (HYSPLIT; Draxler  
179 and Rolph, 2003) model was used to gain insight into the origin of the different  
180 air masses that approach Kyushu. The HYSPLIT model uses a moving frame of  
181 reference for the advection and diffusion calculations, and a fixed three-dimensional  
182 grid as a frame of reference for chemical species concentration calculations. Only  
183 the former was utilised here.

184 The model was used to calculate 5-day backwards trajectories at each sounding  
185 time for one year at one sounding station (2009, Kagoshima station). Trajectories  
186 were modelled at two heights: 1 and 5 km. The National Centers for Environmental  
187 Prediction (NCEP)/National Center for Atmospheric Research (NCAR) reanalysis  
188 dataset was used for all calculations (Kalnay *et al.*, 1996). Note that the trajectory  
189 modelling was used to complement the sounding and rainfall data and the role it  
190 has in the study is mainly informative.

## 191 3 Sounding and air mass characterisation

### 192 3.1 Sounding category specification

193 When categorising different atmospheric states, it is common to use stability pa-  
194 rameters [such as ~~convective available potential energy (CAPE)~~, or the K or Lifted  
195 Index] and water content parameters [such as ~~precipitable water (PW)~~ content], as  
196 their combination is a deciding factor for the type and amount of rainfall on a given  
197 day (McCaul and Weisman, 2001; McCaul and Cohen, 2002; McCaul *et al.*, 2005;  
198 Takemi, 2007a,b, 2014). The categorisation presented here is based on CAPE and  
199 PW for each sounding. The category names were based on the origin and path of  
200 the air masses at different heights (continental, oceanic, and mixed; Figs. 2a–c).  
201 The specific limits specified below for the present study are based on a compromise  
202 between reference values (for example Nishiyama *et al.*, 2007), and the resulting  
203 trajectories and sounding characteristics (presented in Section 3.2). A different  
204 combination of criteria (PW and the wind field at 850 hPa) has also been used  
205 for the prediction of heavy rainfall during the rainy season in Japan (Nishiyama  
206 *et al.*, 2007). Chuda and Niino (2005) showed that CAPE decreases strongly with  
207 latitude (on average Fukuoka has half the CAPE compared to Kagoshima). Thus a  
208 relatively small value for the CAPE limit is used here to distinguish between days  
209 when convection is possible and days that convection is highly unlikely. Note that  
210 due to the large number of trajectory data, results shown in Figs. 2a–c are a subset  
211 for the sake of figure clarity. Trajectory density calculations are based on the entire  
212 dataset.

### 213 **3.1.1 Continental (CNT): Dry; PW<30 mm, any CAPE**

214 Dry soundings were generally associated with both upper and lower air masses orig-  
215 inating from the west, over continental Asia. These sounding are characterised as  
216 “continental” (CNT; Fig. 2a). Averaged trajectories show little variability in the  
217 air masses paths (Figs. 2d,g): The upper air mass indicates an almost completely  
218 westerly wind, while for the lower air masses, the most common path passes from  
219 South Korea and the Sea of Japan. Results here agree with previous trajectory  
220 modelling carried out for Kyushu over the winter season (Kazaoka and Kida, 2006).

### 221 **3.1.2 Oceanic (OCN): Moist and Unstable; PW>30 mm, CAPE>100 J kg<sup>-1</sup>**

222 Moist and unstable soundings were mainly associated with both air masses originat-  
223 ing over the ocean, leading to the characterisation as “oceanic” (OCN; Fig. 2c). In  
224 this case upper air masses mainly originate from the Indian Ocean, while the lower  
225 air masses originated from either the Indian or the Pacific Oceans. Some typhoon  
226 circulations can also be seen in the data, with air masses from both heights circling  
227 east of the station. On average, upper air masses come from a south-westerly point,  
228 with the most common path being over the southern coastline of China (Figs. 2f).  
229 Results for air masses close to the surface are more variable, and the most common  
230 approaches to the station are either from south or the east (Figs. 2i).

### 231 **3.1.3 Mixed (MXD): Moist and Stable; PW>30 mm, CAPE<100 J kg<sup>-1</sup>**

232 Moist and stable soundings were generally seen to belong to an “intermediate” case  
233 and were characterised as “mixed” (MXD; Fig. 2b). In this case, upper air masses

234 approach the station directly from continental Asia passing over the Sea of Japan  
235 (westerly winds with a small south-westerly component; Fig. 2e), while the lower air  
236 masses either originate from the ocean (south or east of Kyushu) or originate from  
237 the continent but pass over central Japan and turn easterly afterwards, becoming  
238 moist as they pass over the Pacific (Fig. 2h).

### 239 **3.1.4** Categorisation criteria limits

240 An effort was made to specify limits that allowed for a categorisation based both  
241 on the limit of the parameter chosen, as well as the origin or path of the air  
242 masses associated [i.e. analysis of the data has shown that *dry* (*moist/unstable*  
243 and *moist/stable*) soundings are generally associated with air masses of *continental*  
244 (*oceanic* and *mixed*) origin]. Even if the strict definition of each category is based  
245 on the thermodynamic structure and water content of the soundings, in the paper  
246 we will be referring to the categories as CNT, OCN, and MXD for ease of language  
247 and because, even if it is not the primary characteristic used to define the categories,  
248 the naming fits the data as seen from the analysis.

249 The categorisation criteria are intentionally simple to allow for a broad and  
250 manageable categorisation of the trajectories and soundings, leading to statistically  
251 significant results. Even though results here are presented for CAPE and PW limits  
252 of  $100 \text{ J kg}^{-1}$  and 30 mm respectively, the qualitative results of the study hold  
253 for CAPE limits between 50–200  $\text{J kg}^{-1}$  and PW limits between 25–40 mm. A  
254 change in the CAPE limit only affects the number of MXD and OCN soundings (an  
255 increased CAPE limit leads to higher number of MXD soundings), while a change in  
256 the PW limit affects the number of CNT and MXD/OCN soundings (an increased

257 PW limit increases the number of CNT soundings, but does not affect the relative  
258 ratio of MXD and OCN soundings). Naturally, the simplicity of the categorisation  
259 criteria leads to some generalisations and overlap: atypical trajectories can be seen  
260 mixed in each category (for example air masses from the continent included in  
261 the OCN soundings). These could be connected with atypical large-scale weather  
262 systems dictating the vertical structure of the soundings. The inclusion of these  
263 soundings does not affect the average soundings to a significant degree; however,  
264 this categorisation should be seen as a first step and each category can easily be  
265 further expanded and studied in more detail.

### 266 **3.1.5 Seasonal distribution**

267 The different sounding categories follow the seasonality of PW and CAPE (Fig. 3).  
268 Averaged over all available stations, there is a notable difference between the peak of  
269 monthly rainfall, which occurs in June due to the rainy season, and average PW and  
270 CAPE, which occur in August due to the typhoon season (Fig. 3a). A secondary  
271 rainfall peak in September is due to the influence of the westerly jet stream (Aizen  
272 *et al.*, 2001). The seasonality of CAPE and PW is consistent with previous results  
273 as noted by Chuda and Niino (2005), and the overall behaviour can be explained in  
274 terms of the large-scale weather systems as discussed in detail in Section 1. Note that  
275 even though on average both PW and CAPE reach a maximum value in August,  
276 the seasonal variation of PW follows a smoother profile, with values over 50% of  
277 the maximum for six months. In contrast, CAPE follows a narrow profile, with the  
278 increased CAPE period limited to 3 months. This relative “lag” between PW and  
279 CAPE is used here to distinguish between the MXD and OCN categories (Fig. 3b).

280 The CNT soundings dominate much of the winter season, however they can  
281 still occur during spring and autumn with a lower frequency. The MXD soundings  
282 can be associated with peaks of monthly rainfall and occur from spring to autumn.  
283 The OCN sounding frequency follow a very similar pattern to the typhoon season  
284 (Goh and Chan, 2012), mainly occurring during the summer with a peak in August.  
285 However that does not mean that typhoons are only related to OCN soundings. The  
286 MXD soundings can also be represent days with stratiform rainfall away from the  
287 convective centre (Uvo *et al.*, 2001; Wang *et al.*, 2009). As noted from the trajectory  
288 analysis, despite some variability, results can be seen as representatives of the early  
289 (MXD) and later (OCN) phases of the Asian Monsoon season and the typhoon  
290 season (Nishiyama *et al.*, 2007).

291 The results for the categorisation are relatively similar for both sounding stations  
292 (Table 1). The CNT category is the most common, covering 60% of the total dataset,  
293 and also exhibits the largest difference between the two stations – Fukuoka (northern  
294 of Kyushu) has 7% more CNT soundings. The MXD category is the second most  
295 common (22% of the total set) and also the least variable. Finally, the OCN category  
296 is the least common and is 5% more likely in Kagoshima (southern Kyushu). This  
297 decrease of the OCN soundings is to be expected due to the decrease of CAPE in  
298 higher latitudes (Chuda and Niino, 2005). For both sets approximately 2% were  
299 unclassifiable as they lacked data or a PW value.

300 The “concurrent” set (final row in Table 1), is used in Section 5. It represents  
301 days when the entire island is categorised by the same sounding type for a day.  
302 Hence, it features a subset of soundings satisfying the following conditions: (i) Same

303 resulting category for both 09 and 21 JST soundings, (ii) Same resulting category  
304 for both Kagoshima and Fukuoka. This is used to ensure that rainfall results can  
305 be linked to a specific atmospheric profile over the whole island. This means that  
306 only 30% of the days are used but it still allows the use of a statistically significant  
307 dataset (3508 days).

### 308 **3.2 Sounding category characteristics**

309 Overall averages of wind direction, wind speed and mixing ratio for the “total”  
310 dataset (all data from both Kagoshima and Fukuoka) reveal complex distributions at  
311 specific heights (Figs. 4a–c). This is to be expected when analysing the dataset as a  
312 whole; however, the complexity persists even if analysed seasonally (not shown here).  
313 The distribution for wind direction is fairly narrow above 800 hPa (approximately  
314 2 km), with an average at 270°, however, in the lower atmosphere it spreads over  
315 the whole range, with increased frequencies at 0–80°, 100–180°, and 270–360°. The  
316 mean profile largely follows the later. Wind speed is narrow at the surface and  
317 becomes wider above a height of 400 hPa ( $\sim 7.5$  km), roughly indicated by the mean  
318 and standard distribution values. This is tied with the seasonal variability of the  
319 subtropical jet stream (Zhang *et al.*, 2006). A similar pattern can be seen for water  
320 vapour mixing ratio: the distribution is wide up to approximately 800 hPa and  
321 becomes progressively narrower with height.

322 Profiles calculated for the three categories using the “total” dataset largely dis-  
323 entangle these distributions (Figs. 4d–f). Specifically, the three profiles follow the  
324 trimodal distributions shown for the wind direction and wind speed very closely. In



325 the case of the wind direction, the results agree with the trajectory analysis pre-  
326 sented in Section 3.1. At low altitudes, CNT is northwesterly, MXD is easterly  
327 to southeasterly, and OCN is southerly. Above 800 hPa all profiles have a strong  
328 westerly component, however OCN shows a small shift towards southerly, as seen  
329 previously. Upper level wind speed reveals the inherent seasonality of the profiles,  
330 as it closely follows the seasonal behaviour of the subtropical jet stream (Zhang  
331 *et al.*, 2006). Below 600 hPa all profiles converge into a single mean value, showing  
332 that the variability in low-level wind is not isolated to a single category. The water  
333 vapour mixing ratio profiles are the least clearly defined: the CNT profile are visibly  
334 differentiated from the MXD and OCN ones, however the MXD and OCN profiles  
335 are relatively similar on average, especially above 600 hPa. The CNT profile closely  
336 follows the peak in the distribution while the MXD and OCN ones are closer to  
337 the upper limits. The data for the profiles are presented in Table 2 as a reference.  
338 The wind shear between the near-surface and mid-tropospheric values is summed  
339 up in Table 3 which shows the surface values and the 850–500 hPa layer means for  
340 different sounding parameters.

341 The characteristics of the three profiles as discussed previously are also confirmed  
342 by the profiles of several sounding parameters (Fig. 5). The CNT and OCN cate-  
343 gories represent the upper and lower limits for all parameters: the average surface  
344 air temperature is approximately 10 and 27°C respectively and the freezing level  
345 increases from 750 hPa for CNT to 580 hPa for OCN (Fig. 5a). The equivalent  
346 potential temperature profiles reveal the inherent stability in the CNT profile, while  
347 show strong instability for OCN (Fig. 5b). In most cases the MXD profile falls in

348 the middle of these two extremes, closer to the OCN category. Despite the relatively  
349 large water vapour mixing ratio difference between the MXD and OCN profiles at  
350 the lower levels, relative humidity (RH) values are very similar (Fig. 5c). This is  
351 due to the difference in the thermal structure of the profiles – the warmer OCN air  
352 can hold larger amounts of water vapour, leading to similar RH values.

353 For each parameter two statistical tests were carried out, comparing each cate-  
354 gory with the others as a whole, per year and per level. All parameters passed the  
355 first two checks; when using all levels the three different categories are statistically  
356 different at a 95–99.9 confidence level. When using specific levels some tests failed:  
357 wind speed at very high levels (150 and 100 hPa) between all categories, and mixing  
358 ratio at 300 and 400 hPa between the MXD and OCN categories. For the majority  
359 of the levels all categories were found to be statistically different from each other,  
360 however it is safer to compare the sounding **as a whole** in order to categorise it.

## 361 **4 Seasonal and annual variation of the sounding** 362 **categories**

363 The frequency of the three profiles has a strong seasonal trend: CNT mainly occurs  
364 from late autumn until early spring, MXD is at its peak frequency in late spring  
365 and early autumn, and OCN is mainly associated with the summer season. This  
366 can be seen in the seasonal characteristics of some specific parameters as well (water  
367 vapour content, wind direction, and upper tropospheric wind speed). Here we will  
368 examine this in more detail by comparing the average profile for each category and

369 the same profile based on season-specific data (Fig. 6).

370 Most profiles exhibit only a small amount of variability even outside of their  
371 “representative” seasons. The sounding category with the least variability is the  
372 OCN (Figs. 6g–i). This is to be expected as it only occurs within a narrow time  
373 frame and the mean OCN profile is close to the summer profile. The largest difference  
374 can be seen for wind direction, where especially close to the surface there is a 90°  
375 shift to easterly between summer and autumn. The CNT and MXD soundings  
376 exhibit similar amounts of variability. Overall, the most variable characteristic is  
377 the wind speed owing to the strong seasonal variability of the subtropical jet stream  
378 (Zhang *et al.*, 2006). Other than that, the MXD soundings are noticeably different  
379 in autumn in the case of wind direction (45–90° more northerly than the average  
380 profile) and in spring in the case of RH (10–20% more humid than the average  
381 profile).

382 The three categories display different amounts of annual variability (Fig. 7).  
383 On average the CNT profiles are the least inter-annually variable: the difference  
384 from the mean value is within 24.5°, 8.5 m s<sup>-1</sup>, and 9.4% for wind direction, wind  
385 speed, and RH respectively. The MXD soundings exhibit the largest amount of  
386 variability in wind direction close to the surface, with a range of over 100°, is reduced  
387 to 28.6° above 800 hPa. Wind speed varies significantly above 400 hPa with a  
388 maximum range of 13.8° at 200 hPa, while RH has similar range to CNT. The OCN  
389 soundings show the largest variability in wind direction (relatively constant range of  
390 approximately 73°) and RH (9.4% close to the surface increasing up to 33% above  
391 600 hPa), however has a relatively small range for wind speed (6.2 m s<sup>-1</sup>).

392 Although not shown here, the temperature profiles exhibit some seasonal varia-  
393 tion as expected (lower temperatures in winter and higher temperatures in the sum-  
394 mer season) with average surface temperatures for CNT ranging between 7–13° C,  
395 MXD between 16–24°C, and OCN 18–26°C, however show little annual variation  
396 (between 1–3°C). The statistical significance of the seasonal and annual variation  
397 from the average for each parameter was checked for each category. All variation  
398 was found to be statistically insignificant at a 95–99.9 confidence level.

## 399 **5 Seasonal variation of rainfall**

400 Here we will study the rainfall patterns in Kyushu depending on season as well as  
401 conditions related to the sounding categories established earlier. For the category-  
402 specific rainfall, only a subset of the rainfall data are used: days when both rawin-  
403 sonde stations are characterised by the same sounding category for both the 0900  
404 and 2100 JST soundings, in order to establish a strong link between the rainfall  
405 and vertical profile, and allow the study of a “quasi-steady-state” rainfall response.  
406 This is referred to as the “concurrent” set. Due to this selection tends to exclude  
407 “transitional” rainfall episodes. For example during the Baiu season some times  
408 accumulated high values of CAPE are found in the south and neutral conditions  
409 on the north after the CAPE has been released due to rainfall, leading to a mix of  
410 convective and non-convective rainfall respectively (Akiyama, 1978). Although this  
411 plays an important role in the long-term climatological behaviour of the rainfall, a  
412 detailed analysis is outside the general scope of this study, but will be considered in  
413 future work.

414 Daily rainfall distribution shows strong seasonal variability (Fig. 8). During  
415 winter, with the exception of the Yakushima island in the south of Kyushu, rainfall  
416 is limited to an average of 0–2.5 mm day<sup>-1</sup> in the north and up to 5 mm day<sup>-1</sup> in  
417 the south. This is due to the different paths the air masses follow: in the north,  
418 air passes through the Korea and Tsushima Straits obtaining a smaller amount  
419 of moisture, while in the south air masses follow a more favourable path for the  
420 moisture transport over the East China Sea (Uvo *et al.*, 2001). The northern part  
421 of the Yakushima island (30.35°N, 130.53°E) receives more than double the average  
422 precipitation (7.5–10 mm day<sup>-1</sup>) compared to both the rest of stations in Kyushu  
423 and the nearby islands, as well as the southern part of the same island. Rainfall  
424 during spring and autumn are relatively similar, with average daily rainfall ranging  
425 between 5–10 mm day<sup>-1</sup> at southern and south-eastern part of the island; however,  
426 during autumn there is a shift towards a more eastern distribution due to the passage  
427 of typhoons (Uvo *et al.*, 2001). During the summer season, the island receives the  
428 most precipitation with average daily rainfall values more than 10 mm day<sup>-1</sup>. Heavy  
429 rainfall is concentrated on the central, southern, and eastern parts of the island  
430 ( $R_d > 10$  mm day<sup>-1</sup>), while rainfall peaks are mainly concentrated in the central  
431 part of the island.

432 Different rainfall patterns are now examined for each sounding category (Fig.  
433 9). Barring some differences in magnitude, rainfall pattern per sounding category  
434 show similarities with rainfall patterns per season, specifically CNT with winter,  
435 MXD with spring and autumn, and OCN with summer. The differences in mag-  
436 nitude can be expected as different seasons can be characterised by a combination

437 of sounding categories (for example spring has an almost equal number of CNT  
438 and MXD soundings). The CNT profile closely match the winter rainfall pattern  
439 in both distribution and magnitude, as most of the winter season is comprised of  
440 CNT-type soundings. The MXD category rainfall distributions resemble the spring  
441 and autumn distribution, with rainfall focused mainly over the southern and south-  
442 western part of the island, however the daily rainfall values are different, affected  
443 by the CNT-type days.

444 The MXD profile features the largest daily rainfall values: the southern part of  
445 the island sees rainfall over  $18 \text{ mm day}^{-1}$ , while stations along the eastern coast  
446 record rainfall over  $24 \text{ mm day}^{-1}$ . Considering that this profile is specifically chosen  
447 to have less than  $100 \text{ J kg}^{-1}$  of CAPE, and this continues for the whole day, two  
448 assumptions can be made: either it is non-convective, frontal rainfall, or typhoon-  
449 related rainfall as a large amount of water vapour is pushed towards the island in a  
450 western–northwestern flow (Uvo *et al.*, 2001; Wang *et al.*, 2009).

451 For the OCN category, rainfall is mainly concentrated in the middle of the island,  
452 pointing towards strong orographic triggering of rainfall (Houze, 2012). This is to  
453 be expected, as the OCN profiles, satisfy the conditions prescribed by Lin *et al.*  
454 (2001) for heavy orographic precipitation. The distribution of rainfall has similarities  
455 with that presented by Unuma and Takemi (2016), for the distribution of quasi-  
456 stationary convective systems. The OCN distribution partially resembles the rainfall  
457 distribution over the summer season in Fig. 8. When looking at the season as a  
458 whole, rainfall patterns are the results of both the OCN and the MXD categories.

459 All categories include some days with atypical rainfall patterns, however overall

460 the OCN category has the most variable rainfall response. For example these are  
461 days when the CAPE-release mechanism from south to north described previously  
462 (Akiyama, 1978) has not led to a decrease of CAPE below  $100 \text{ J kg}^{-1}$ . On these days  
463 the rainfall response looks similar to a MXD day with a gradual decrease of daily  
464 rainfall towards the north. Aside from that, there are also days with orographic  
465 rainfall over some parts (south or north), days with the Nagasaki or Koshikijima  
466 lines, as well as days with strong rainfall over the whole island. However these  
467 atypical responses get averaged out in the final pattern and the *average response* is  
468 an orographic rainfall regime.

469 The statistical significance of the difference in the rainfall response for each  
470 category was checked for: all data, per year, and per station. When using the dis-  
471 tributions as a whole or when comparing data per year, all categories were found  
472 to have a statistically significantly different response. When comparing data per  
473 station, a number of stations failed the test between the MXD and OCN categories  
474 (for example stations in the north-west part of the island or ones located on moun-  
475 tains). Similarly to the vertical profiles discussed in Section 3.2, when categorising  
476 the rainfall response it is suggested to use as many stations as possible to get a  
477 statistically significant result.

478 The relation between the topography and resulting rainfall is shown in Figure 10,  
479 both for daily and peak rainfall. Strong orographic forcing can be seen in the case of  
480 the OCN category, where large values of both daily rainfall and rainfall intensity are  
481 seen for large station heights. This is partially true for the MXD sounding as well,  
482 although the orographic effect is clearly less important. The pattern previously seen

483 for the MXD rainfall is reflected in the latitude and longitude scatter plots (Figs.  
484 10b,c and 10e,f): large amounts of rainfall occur to the east ( $\text{LON} > 130^\circ$ ) and the  
485 south ( $\text{LAT} < 33^\circ$ ). Specifically in the south-north alignment the increase in rainfall is  
486 almost linear. For OCN, large amounts of rainfall are typically limited in the middle  
487 of both ranges, following the island topography. Results for the CNT category show  
488 that rainfall is generally distributed evenly across the island with some elements  
489 of orographically-forced rainfall and an increase towards the south. On average,  
490 MXD soundings lead to larger daily rainfall but lower peak rainfall (non-convective  
491 rainfall), compared to the OCN soundings (convective rainfall). Results agree with  
492 the seasonal analysis presented by Uvo *et al.* (2001).

493 Histograms of rainfall reveal a similar distribution between the MXD and OCN  
494 categories (Fig. 11). When each individual value from the whole dataset is included,  
495 rainfall rate frequency decreases almost exponentially for increased rates. The peak  
496 in the rainfall distribution for all three categories is at  $0\text{--}5 \text{ mm day}^{-1}$  for daily rainfall  
497 and  $0\text{--}2 \text{ mm (10 min)}^{-1}$  for the peak rainfall intensity. For daily rainfall, the CNT  
498 category shows the largest decrease, and while the MXD and OCN categories are  
499 similar, MXD consistently has a higher frequency. Averaged over the 16-year period  
500 for each station this leads to similar distributions for the two categories with the  
501 same peak averaged daily rainfall. However, in the MXD case the distribution trails  
502 more towards the higher values, leading to a larger overall average (Figs. 11a,b  
503 and Table 4). The opposite is true for daily peak rainfall intensity, here the OCN  
504 category has consistently higher values, leading to different peak frequencies and a  
505 higher average peak rainfall intensity (Figs. 11c,d and Table 4).



506 Average values of stability criteria allow for a quick summary of each category  
507 (Table 4). The CNT category represents cold, dry air masses from continental Asia  
508 do not have enough time to gather moisture east of Kyushu. The result is very  
509 strong atmospheric stability reflected in all parameters, with little to no rainfall  
510 generated as a result. The MXD category usually involves cold and dry air masses  
511 for the west mixing with moist, warmer air masses from the Pacific. This leads to  
512 large amounts of non-convective rainfall, with smaller peak rainfall rates but large  
513 overall rainfall per day, most likely caused by mid-latitude synoptic cyclones and the  
514 Baiu stationary front or by typhoon-forced circulation (Uvo *et al.*, 2001). Finally,  
515 the OCN category represents the warm, moist oceanic air masses either from the  
516 Indian or the Pacific Ocean. These exhibit low atmospheric stability and rainfall is  
517 convective and shows evidence of orographical triggering, leading to shorter duration  
518 but higher peak rainfall intensity. Although not shown here, using data from all  
519 stations (including statistically “compromised” stations) led to a 0.1–3.5% change  
520 in the final rainfall values.

## 521 **6 Summary and conclusions**

522 Rawinsonde data were used to study the seasonality of the weather in the island of  
523 Kyushu in southern Japan over a 16-year study period. In the past a climatological  
524 analysis has been carried out across Japan by Chuda and Niino (2005) studying  
525 the seasonal variation of several mesoscale parameters including PW and CAPE.  
526 Here the vertical structure of the atmosphere was studied and the analysis was  
527 focused on distinguishing the different atmospheric sounding categories that are

528 tied to the seasonal climatological behaviour. Data from the rawinsondes along  
529 with air mass trajectories revealed three distinct categories, based on water content  
530 (a PW threshold of 30 mm) and stability (a CAPE threshold of  $100 \text{ J kg}^{-1}$ ) criteria,  
531 as well as air mass origins: the dry, stable air masses that originate from continental  
532 Asia and occur mainly during winter (CNT), the moist, unstable air masses that  
533 originate from the Indian or the Pacific oceans (OCN), and an intermediate, mixed,  
534 case when upper air masses from the continent mix with air masses passing over  
535 the Pacific (MXD). Vertical profiles based on the three categories were found to be  
536 statistically robust and were seen to disentangle the complex distributions of the  
537 several atmospheric parameters. The annual variability in the characteristics of the  
538 sounding categories calculated here was seen to be sufficiently small, as to allow the  
539 long-term use of the study's results.

540 The rainfall response over Kyushu for each category was also studied using rain-  
541 fall data from the AMeDAS network of the Japan Meteorological Agency. Based  
542 on the particular characteristics of each sounding category, a distinct rainfall re-  
543 sponse was noted: very low amounts of rainfall in the CNT case, high amounts of  
544 non-convective rainfall in the MXD case, and high amounts of convective rainfall  
545 in the OCN case. Average daily rainfall rates are similar for the MXD and OCN  
546 categories, but peak rainfall rates are higher in the OCN case. Parallels in the rain-  
547 fall response for each category were also drawn between the seasonal variation of  
548 rainfall patterns and the frequency of occurrence for each sounding category: the  
549 rainfall patterns over the winter season corresponded to the CNT case, spring and  
550 autumn was the combined effect of the CNT and MXD settings, while rainfall over

551 the summer corresponded to a combination of the OCN and MXD profiles.

552 The results from this study represent the first effort to create average atmospheric  
553 profiles in this region. It is our hope that they will be used and expanded upon in  
554 the future to help enhance our understanding of the climatological variability in the  
555 area, as well as help in the study and modelling of atmospheric natural hazards in  
556 the Kyushu area as well as the extended region. The study focused mainly on the use  
557 of observational data, using modelling only to fill in some gaps in observational data  
558 (humidity-based parameters over a height of 400 hPa), and for trajectory modelling,  
559 which was used mainly to gain a general insight on the air masses. Numerical  
560 weather prediction model capability of reproducing the results found here will be  
561 tested in the future in long, climatological simulations. Finally, the capability of  
562 the averaged vertical profiles to reproduce the rainfall patterns discussed here and  
563 to replicate known volcanic ash dispersal patterns from the Sakurajima volcano will  
564 also be tested in an idealised setting.

## 565 **7 Acknowledgements**

566 Alexandros P. Poulidis was funded by the Japan Society for the Promotion of Sci-  
567 ences (JSPS). The authors would like to thank Ian Renfrew and Takashi Unuma  
568 for comments on the manuscript draft and useful discussions and two anonymous  
569 reviewers for the helpful comments. All data analysis was carried out using Matlab.

## 570 **References**

- 571 Ackermann P. 1997. The four seasons. *Japanese images of nature: Cultural perspec-*  
572 *tives* : 36.
- 573 Aizen EM, Aizen VB, Melack JM, Nakamura T, Ohta T. 2001. Precipitation and  
574 atmospheric circulation patterns at mid-latitudes of Asia. *Int. J. Climatol.* **21**(5):  
575 535–556, doi:10.1002/joc.626.
- 576 Akiyama T. 1978. Mesoscale pulsation of convective rain in medium-scale dis-  
577 turbances developed in Baiu front. *J. Meteorol. Soc. Japan* **56**: 448–451.
- 578 Barclay J, Johnstone JE, Matthews AJ. 2006. Meteorological monitoring of an active  
579 volcano: Implications for eruption prediction. *J. Volcanol. Geoth. Res.* **150**: 339–  
580 358, doi:10.1016/j.jvolgeores.2005.07.020.
- 581 Bluestein HB, Jain MH. 1985. Formation of mesoscale lines of precipitation: Severe  
582 squall lines in Oklahoma during the spring. *J. Atmos. Sci.* **42**(16): 1711–1732.
- 583 Bonadonna C, Folch A, Loughlin S, Puempel H. 2012. Future developments in mod-  
584 elling and monitoring of volcanic ash clouds: outcomes from the first IAVCEI-  
585 WMO workshop on Ash Dispersal Forecast and Civil Aviation. *Bull. Volcanol.*  
586 **74**: 1–10, doi:10.1007/s00445-011-0508-6.
- 587 Carn SA, Watts RB, Thompson G, Norton GE. 2004. Anatomy of a lava dome  
588 collapse: The 20 march 2000 event at Soufrière Hills Volcano, Montserrat. *J.*  
589 *Volcanol. Geoth. Res.* **131**: 241–264, doi:10.1016/S0377-0273(03)00364-0.
- 590 Chuda T, Niino H. 2005. Climatology of environmental parameters for mesoscale

591 convections in Japan. *J. Meteorol. Soc. Japan* **83**(3): 391–408, doi:  
592 10.2151/jmsj.83.391.

593 Dee DP, Uppala SM, Simmons AJ, Berrisford P, Poli P, Kobayashi S, Andrae U,  
594 Balmaseda MA, Balsamo G, Bauer P, Bechtold P, Beljaars ACM, van de Berg L,  
595 Bidlot J, Bormann N, Delsol C, Dragani R, Fuentes M, Geer AJ, Haimberger L,  
596 Healy SB, Hersbach H, Holm EV, Isaksen L, Kallberg P, Kohler M, Matricardi  
597 M, McNally AP, Monge-Sanz BM, Morcrette JJ, Park BK, Peubey C, de Rosnay  
598 P, Tavolato C, Thepaut JN, Vitart F. 2011. The ERA-Interim reanalysis: Config-  
599 uration and performance of the data assimilation system. *Q. J. R. Meteorol. Soc.*  
600 **137**(656): 553–597, doi:10.1002/qj.828.

601 Draxler RR, Rolph GD. 2003. HYSPLIT (HYbrid Single-Particle Lagrangian Inte-  
602 grated Trajectory) model access via NOAA ARL READY website. NOAA Air Re-  
603 sources Laboratory, Silver Spring. <http://www.arl.noaa.gov/ready/hysplit4.html>,  
604 Accessed: 2016-03-11.

605 Dunion J. 2011. Rewriting the climatology of the tropical North At-  
606 lantic and Caribbean Sea atmosphere. *J. Clim.* **24**(3): 893–908, doi:  
607 10.1175/2010JCLI3496.1.

608 Goh AZC, Chan JCL. 2012. Variations and prediction of the annual number of  
609 tropical cyclones affecting Korea and Japan. *Int. J. Climatol.* **32**(2): 178–189,  
610 doi:10.1002/joc.2258.

611 Gray WM. 1968. Global view of the origin of tropical disturbances and storms. *Mon.*  
612 *Weather Rev.* **96**(10): 669–700.

613 Grossman MJ, Zaiki M, Nagata R. 2014. Interannual and interdecadal varia-  
614 tions in typhoon tracks around Japan. *Int. J. Climatol.* **2527**: 2514–2527, doi:  
615 10.1002/joc.4156.

616 Hillman SE, Horwell CJ, Densmore AL, Damby DE, Fubini B, Ishimine Y, Tomatis  
617 M. 2012. Sakurajima volcano: a physico-chemical study of the health consequences  
618 of long-term exposure to volcanic ash. *Bull. Volcanol.* **74**: 913–930.

619 Houze RA. 2012. Orographic effects on precipitating clouds. *Rev. Geophys.* **50**, doi:  
620 10.1029/2011RG000365.

621 Houze Jr RA. 1997. Stratiform precipitation in regions of convection: A meteo-  
622 rological paradox? *Bull. Am. Meteor. Soc.* **78**: 2179–2196, doi:10.1175/1520-  
623 0477(1997)078<2179:SPIROC>2.0.CO;2.

624 Iguchi M. 2016. Method for real-time evaluation of discharge rate of volcanic ash  
625 - Case study on intermittent eruptions at the Sakurajima volcano, Japan -. *J.*  
626 *Disaster Res.* **11**: 4–14, doi:10.20965/jdr.2016.p0004.

627 Iwasaki H. 2014. Increasing trends in heavy rain during the warm season in eastern  
628 Japan and its relation to moisture variation and topographic convergence. *Int. J.*  
629 *Climatol.* **2163**: 2154–2163, doi:10.1002/joc.4115.

630 Kalnay E, Kanamitsu M, Kistler R, Collins W, Deaven D, Gandin L, Iredell M, Saha  
631 S, White G, Woollen J, Zhu Y, Leetmaa A, Reynolds R, Chelliah M, Ebisuzaki  
632 W, Higgins W, Janowiak J, Mo KC, Ropelewsji C, Wang J, Jenne R, Joseph D.  
633 1996. The NCEP/NCAR 40-year reanalysis project. *Bull. Am. Meteorol. Soc.* **77**:  
634 437–471.

- 635 Kato T. 2005. Statistical study of band-shaped rainfall systems, the Koshikijima and  
636 Nagasaki lines, observed around Kyushu island, Japan. *J. Meteorol. Soc. Japan*  
637 **83**(6): 943–957, doi:10.2151/jmsj.83.943.
- 638 Kazaoka R, Kida H. 2006. Characteristic Transport Route of Air Parcels Arriving  
639 over Northern Japan in January. *Sola* **2**: 172–175, doi:10.2151/sola.2006-044.
- 640 Lau KM, Sheu PJ. 1988. Annual cycle, quasi-biennial oscillation, and south-  
641 ern oscillation in global precipitation. *J. Geophys. Res.* **93**: 10 975–10 988, doi:  
642 10.1029/JD093iD09p10975.
- 643 Lin YL, Chiao S, Wang TA, Kaplan ML, Weglarz RP. 2001. Some common in-  
644 gredients for heavy orographic rainfall. *Weather Forecast.* **16**(6): 633–660, doi:  
645 10.1175/1520-0434(2001)016<0633:SCIFHO>2.0.CO;2.
- 646 Mastin LG. 1994. Explosive tephra emissions at Mount St. Helens. 1989–1991: The  
647 violent escape of magmatic gas following storms? *Geol. Soc. Am. Bull.* **106**: 175–  
648 185, doi:10.1130/0016-7606(1994)106,0175:ETEAMS.2.3.CO;2.
- 649 Matthews AJ, Barclay J, Carn S, Thompson G, Alexander J, Herd R, Williams C.  
650 2002. Rainfall-induced volcanic activity in Montserrat. *Geophys. Res. Lett.* (13):  
651 1–4, doi:10.1029/2002GL014863.
- 652 McCaul EWJ, Cohen C. 2002. The impact on simulated storm structure and inten-  
653 sity of variations in the mixed layer and moist layer depths. *Mon. Weather. Rev.*  
654 **130**: 1722–1748.
- 655 McCaul EWJ, Cohen C, Kirkpatrick C. 2005. The sensitivity of simulated storm

656 structure, intensity, and precipitation efficiency to environmental temperature.  
657 *Mon. Weather. Rev.* **133**: 3015–3037.

658 McCaul EWJ, Weisman ML. 2001. The sensitivity of simulated supercell structure  
659 and intensity to variations in the shapes of environmental buoyancy and shear  
660 profiles. *Mon. Weather. Rev.* **129**: 664–687.

661 Miyabuchi Y, Daimaru H, Komatsu Y. 2004. Landslides and lahars triggered by  
662 the rainstorm of June 29, 2001, at Aso Volcano, Southwestern Japan. *Chikei* **25**:  
663 23–43.

664 Ninomiya K, Yamazaki K. 1979. Heavy rainfalls associated with frontal depression  
665 in Asian subtropical humid region (II) Mesoscale features of precipitation, radar  
666 echoes and stratification. *J. Meteorol. Soc. Japan* **57**: 399–412.

667 Nishiyama K, Endo S, Jinno K, Uvo CB, Olsson J, Berndtsson R. 2007. Identi-  
668 fication of typical synoptic patterns causing heavy rainfall in the rainy season  
669 in Japan by a Self-Organizing Map. *Atmos. Res.* **83**(2-4 SPEC. ISS.): 185–200,  
670 doi:10.1016/j.atmosres.2005.10.015.

671 Takemi T. 2007a. A sensitivity of squall-line intensity to environmental static sta-  
672 bility under various shear and moisture conditions. *Atmos. Res.* **84**(4): 374–389,  
673 doi:10.1016/j.atmosres.2006.10.001.

674 Takemi T. 2007b. Environmental stability control of the intensity of squall  
675 lines under low-level shear conditions. *J. Geophys. Res.* **112**: D24110, doi:  
676 10.1029/2007JD008793.



- 677 Takemi T. 2014. Convection and precipitation under various stability and shear  
678 conditions: Squall lines in tropical versus midlatitude environment. *Atmos. Res.*  
679 **142**: 111–123, doi:10.1016/j.atmosres.2013.07.010.
- 680 Unuma T, Takemi T. 2016. Characteristics and environmental conditions of quasi-  
681 stationary convective clusters during the warm season in Japan. *Q. J. R. Meteorol.*  
682 *Soc.* doi:10.1002/qj.2726.
- 683 Uvo CB, Olsson J, Morita O, Jinno K, Kawamura A, Nishiyama K, Koreeda N,  
684 Nakashima T. 2001. Statistical atmospheric downscaling for rainfall estimation in  
685 Kyushu Island, Japan. *Hydrol. Earth Syst. Sci.* **5**(2): 259–271, doi:10.5194/hess-  
686 5-259-2001.
- 687 Wang B, Ho L. 2002. Rainy season of the asian-pacific summer monsoon. *J. Clim.*  
688 **15**: 386–398, doi:10.1175/1520-0442(2002)015<0386:RSOTAP>2.0.CO;2.
- 689 Wang Y, Wang Y, Fudeyasu H. 2009. The role of Typhoon Songda (2004) in produc-  
690 ing distantly located heavy rainfall in Japan. *Mon. Weather Rev.* **137**: 3699–3716,  
691 doi:10.1175/2009MWR2933.1.
- 692 Wilson TM, Stewart C, Sword-Daniels V, Leonard GS, Johnston DM, Cole JW,  
693 Wardman J, Wilson G, Barnard ST. 2012. Volcanic ash impacts on critical in-  
694 frastructure. *Physics and Chemistry of the Earth, Parts A/B/C* **45**: 5–23, doi:  
695 10.1016/j.pce.2011.06.006.
- 696 Yamasato J, Kitagawa S, Komiya M. 1998. Effect of rainfall on dacitic lava dome  
697 collapse at Unzen volcano, Japan. *Pap. Meteorol. Geophys.* **48**(3): 73–78.

- 698 Yoshizaki M, Kato T, Tanaka Y, Shoji Y, Seko H, Arao K, Kazuo M. 2000. Analytical  
699 and numerical study of the 26 June 1998 orographic rainband observed in western  
700 Kyushu, Japan. *J. Meteorol. Soc. Japan* **78**(6): 835–856.
- 701 Zhang Y, Kuang X, Guo W, Zhou T. 2006. Seasonal evolution of the upper-  
702 tropospheric westerly jet core over East Asia. *Geophys. Res. Lett.* **33**(11): 3–6.

703 8 Figures

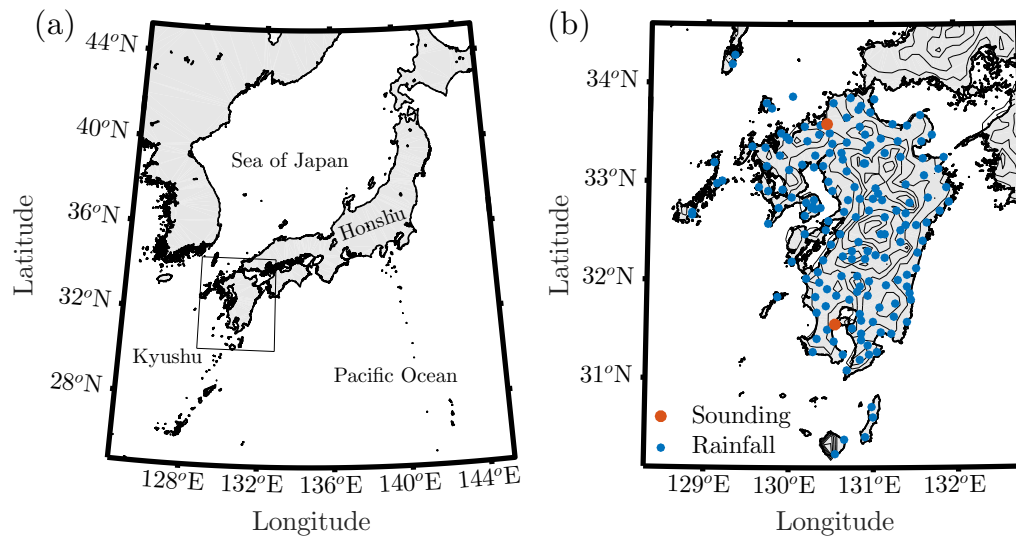


Figure 1: (a) Map of Kyushu and the surrounding area. (b) Locations of “Sounding” stations (red; provide both sounding and rainfall data) and “rainfall” (AMeDAS) stations (blue; only provide rainfall data). Height contours start at 100 m and every 200 m after.

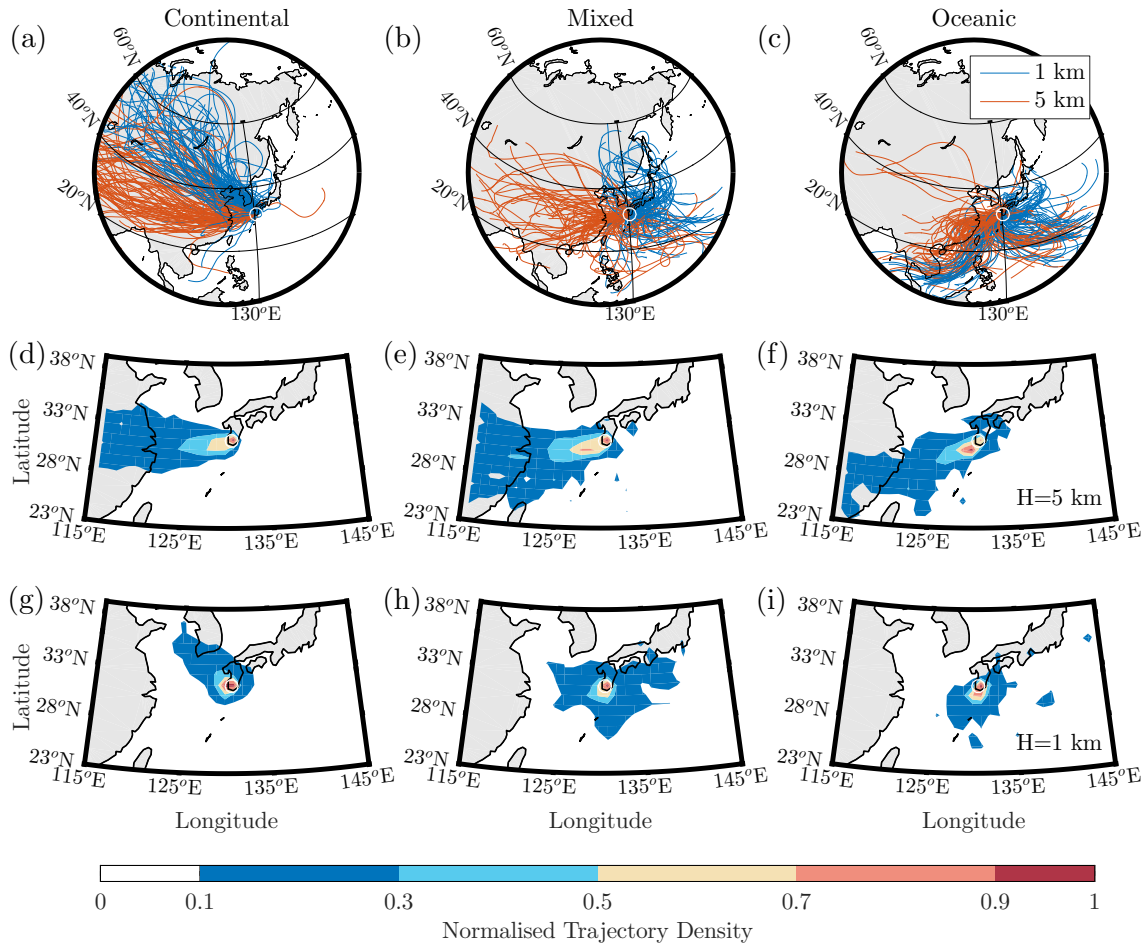


Figure 2: Subset of the five-day back trajectories for: (a) Continental (CNT), (b) Mixed (MXD), and (c) Oceanic (OCN) air masses for that were identified at 0900 and 2100 JST (0000 and 1200 UTC) throughout 2009. Normalised trajectory density (calculated for all 2009 data) is shown for: (d)–(f) all categories at 5 km, and (g)–(i) all categories at 1 km. The trajectories were calculated using the HYSPLIT model, at 1 and 5 km (blue and red lines respectively at Panels a–c) originating from the Kagoshima sounding station (white circle). Trajectory density was calculated at a  $1^\circ$  resolution.

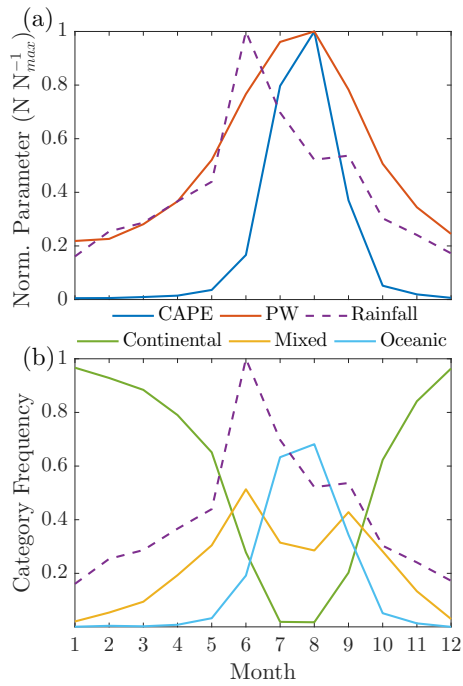


Figure 3: (a) Average normalised values of monthly rainfall intensity, CAPE, and PW for every month from 1998–2013. (b) Frequency of occurrence of each sounding category and normalised rainfall per month.

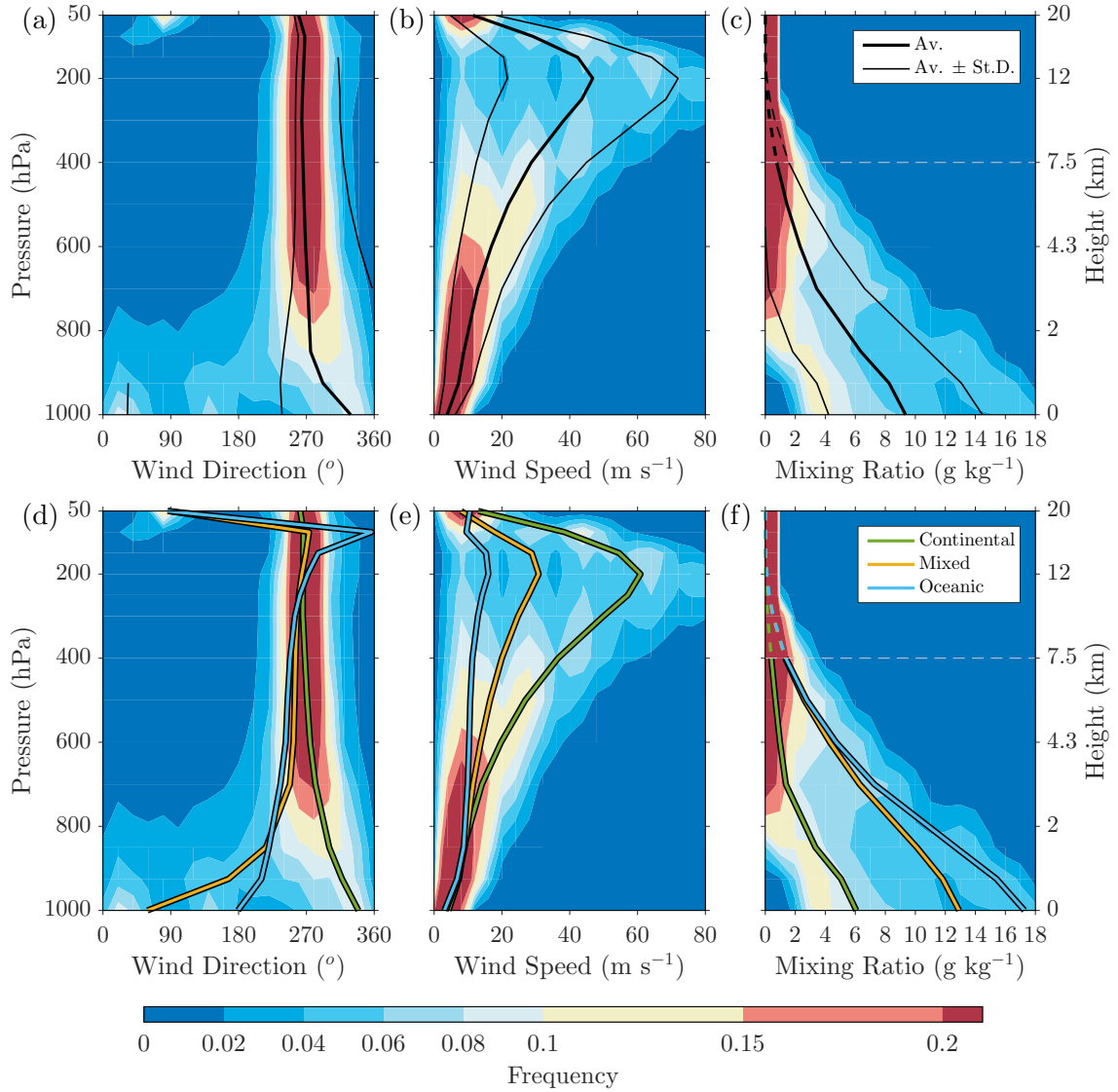


Figure 4: Contoured frequency by altitude diagrams of (a),(d) Wind direction, (b),(e) Wind speed, and (c), (f) Water vapour mixing ratio, overlaid with the combined 16-year average (i.e. all sounding data) and average plus/minus one standard deviation [(a)–(c)], and the 16-year averages for the CNT, MXD, and OCN sounding types [(d)–(f)]. Frequency of occurrence bins were calculated at each level using bin sizes of  $20^\circ$ ,  $5 \text{ m s}^{-1}$ , and  $1 \text{ g kg}^{-1}$ , respectively. Water vapour mixing ratio data above 400 hPa (dashed) were estimated using ECMWF Era-Interim data.

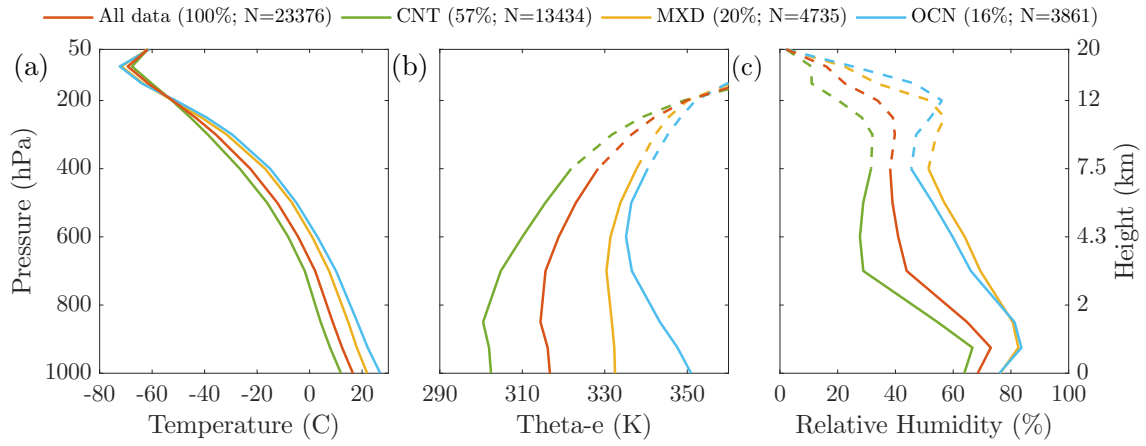


Figure 5: Mean sounding parameters for each sounding category, and the combined average across the study period (1998-2013): (a) Temperature, (b) Equivalent potential temperature, (c) Relative humidity. In the legend, numbers in brackets indicate the percentage and total number of soundings per category.

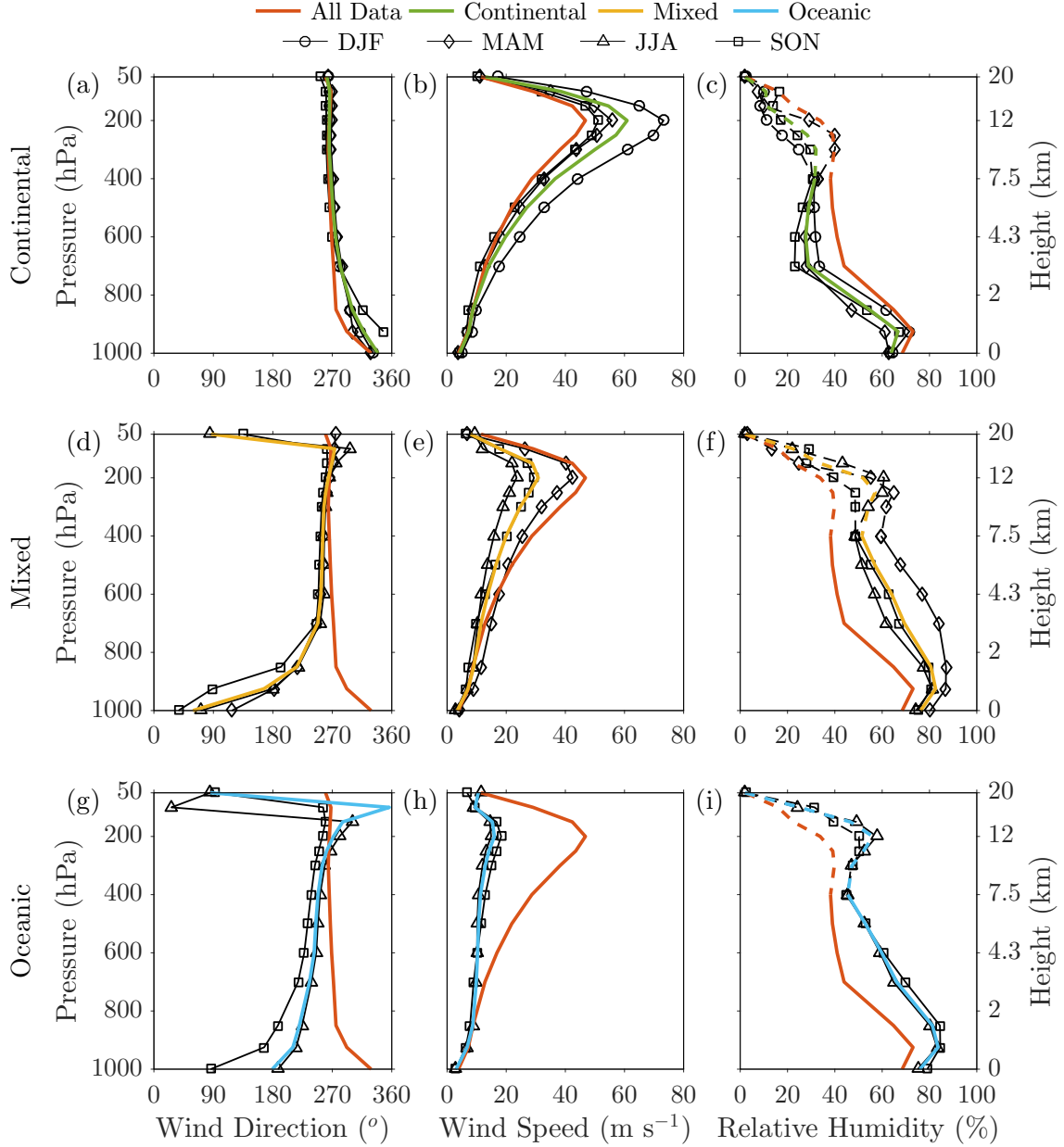


Figure 6: Average wind direction (first column), wind speed (second column), and relative humidity (third column) for: (a)–(c) CNT, (d)–(f) MXD, and (g)–(i) OCN soundings, for the whole data range, as well as each season per category, and the combined average. Note that some seasonal data are not presented for each category (summer for CNT, winter for MXD and OCN, and spring for OCN), due to the small number of sounding data ( $< 5\%$  of the total number per category).



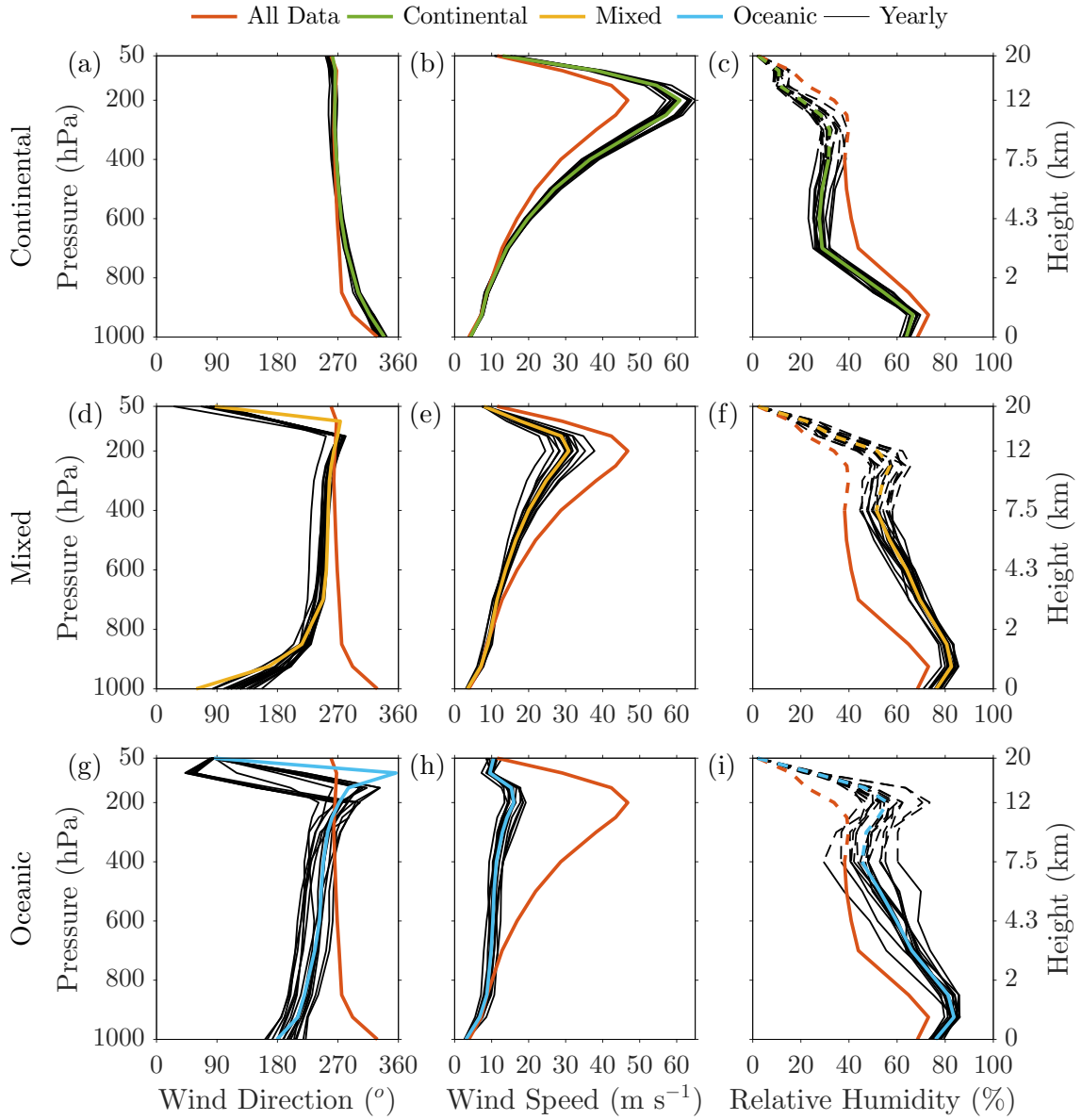


Figure 7: As Fig. 6 but with individual years from 1998-2013, and the combined average.

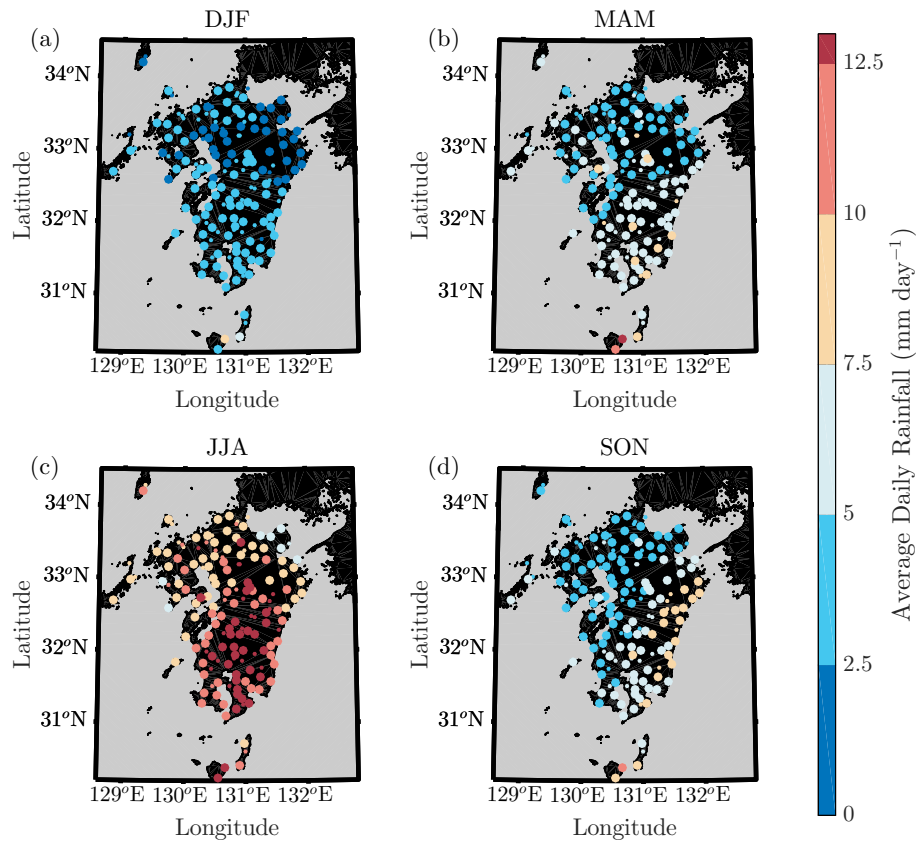


Figure 8: Combined average of daily rainfall over Kyushu for: (a) Winter, (b) Spring, (c) Summer, and (d) Autumn, for all days from 1998-2013. Based on a subset of days with the same sounding category for 0900 and 2100 JST, over both Kagoshima and Fukuoka (“concurrent”). Small dots signify statistically “compromised” stations (provide data for less than 90% of the study period).

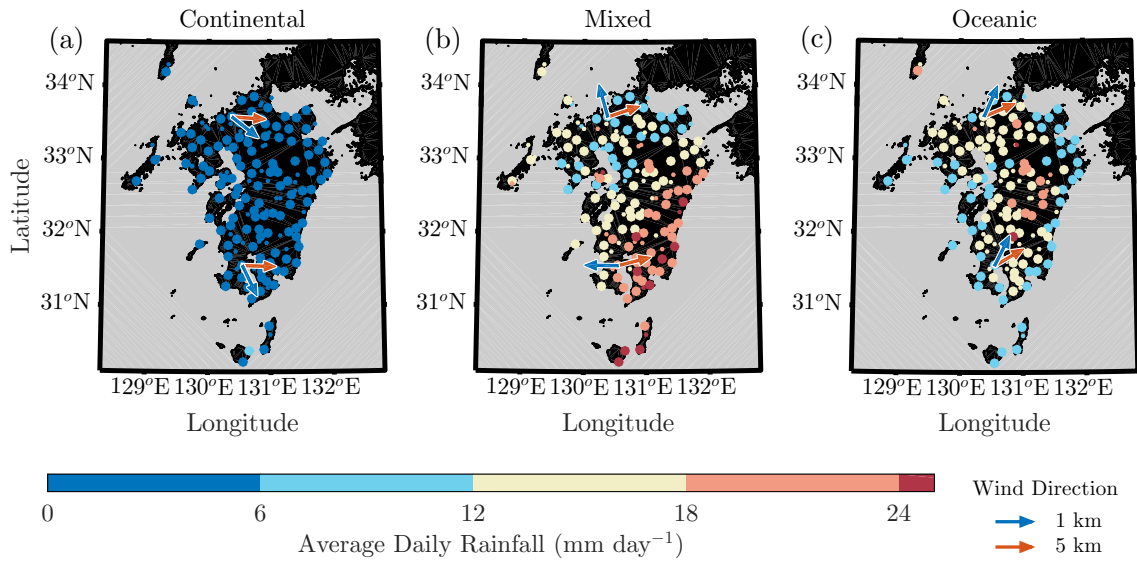


Figure 9: Average daily rainfall over Kyushu for: (a) CNT, (b) MXD, and (c) OCN. Arrows indicate average wind direction at 5 and 1 km over each station. Small dots signify statistically “compromised” stations (provide data for less than 90% of the study period).

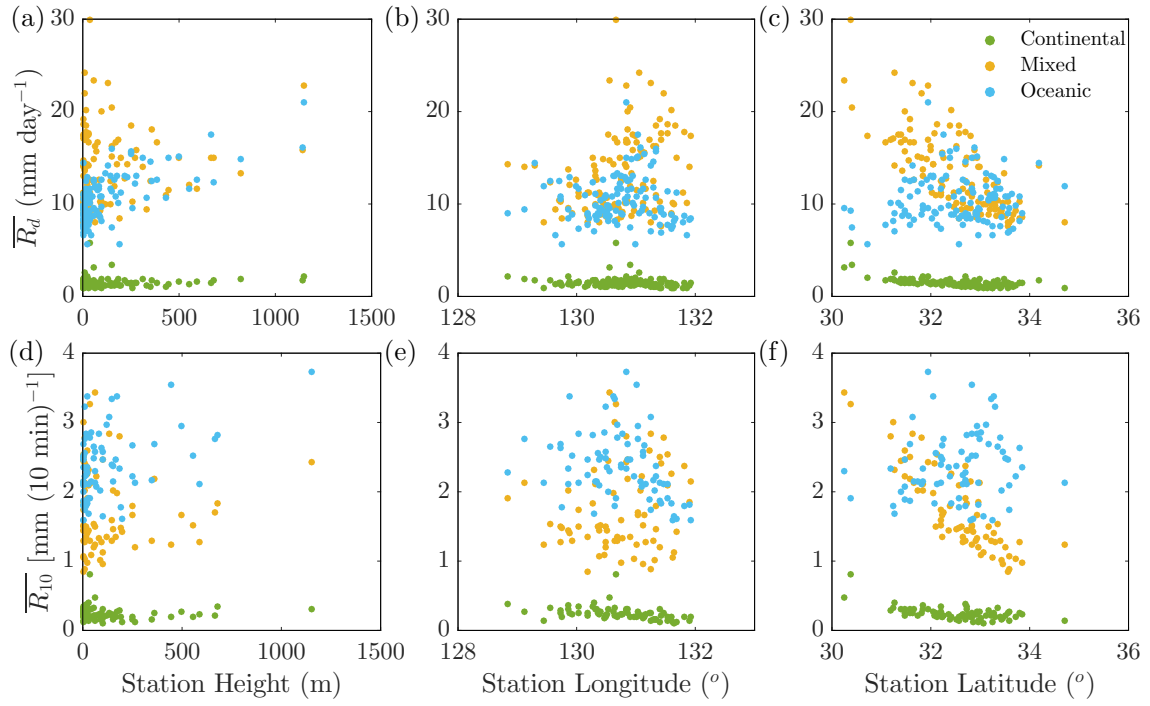


Figure 10: Scatter plots of average daily rainfall (Panels a–c) and peak rainfall intensity (Panels d–f) against: (a,d) Station height, (b,e) Station longitude, and (c,f) Station latitude, for all sounding categories for the “concurrent” days subset. Only statistically significant data are shown.

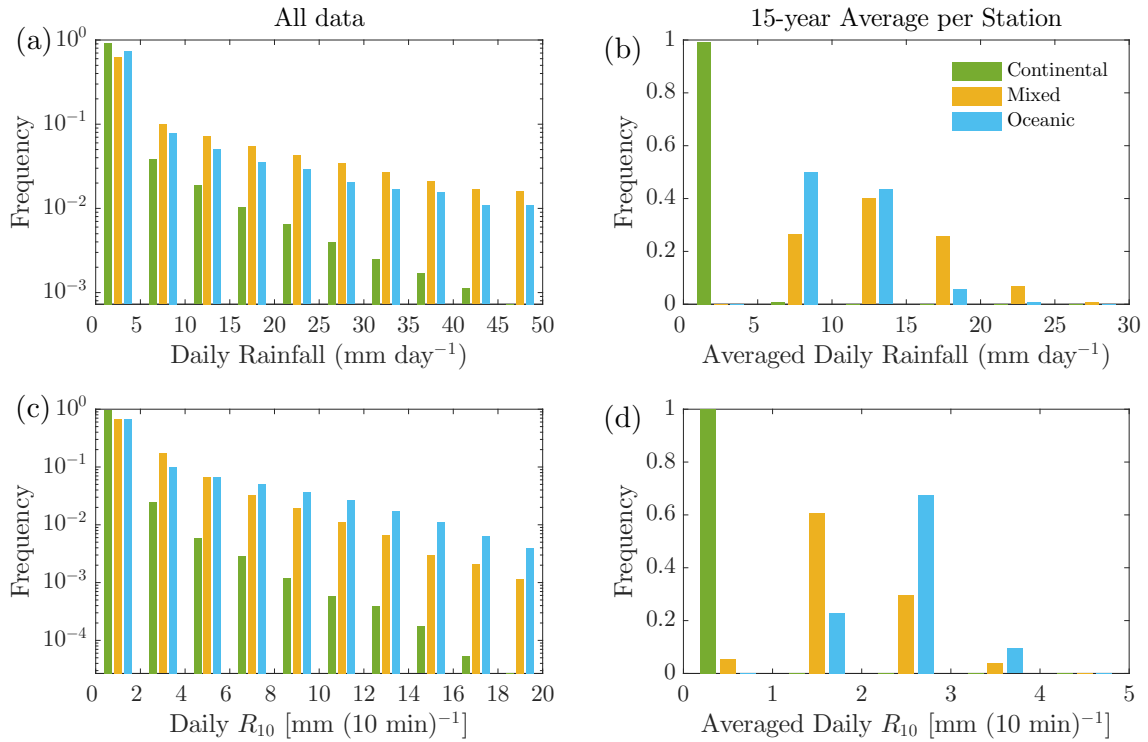


Figure 11: Histograms for: (a,b) Daily rainfall and (c,d) Peak rainfall intensity, for all sounding categories in the “concurrent” days subset. Panels a and c use all available daily data without any averaging (714240 data points in total), while panels b and d use the 16-year averages for every station (120 data points). Only statistically significant data are used for the calculations. Note the logarithmic scale in Panels a and c.

## 9 Tables

Table 1: Total number ( $N$ ) and frequency of occurrence ( $f$ ) for each sounding category. “UNC” stands for *unclassifiable*. In the last row, the values outside of the brackets are with respect to the total number of “concurrent” soundings, while the values in the brackets are with respect to the total number of soundings.

Station	Total	$N_{CNT}$	$f_{CNT}$	$N_{MXD}$	$f_{MXD}$	$N_{OCN}$	$f_{OCN}$	$N_{UNC}$	$f_{UNC}$
Kagoshima	11688	6272	0.54	2448	0.21	2278	0.19	690	0.06
Fukuoka	11688	7162	0.56	2278	0.20	1583	0.14	656	0.06
Total	23376	13434	0.57	4735	0.20	3861	0.16	1346	0.06
Concurrent	3106	2231	0.72	490	0.16	385	0.12	105(8582)	0.03(0.73)

Table 2: CNT (first row), MXD (second row), OCN (third row), and all sounding (fourth row, bold) mean atmospheric soundings (1998-2013). Data in italics are estimates based on the ECMWF ERA-Interim reanalysis dataset.

$P$ (hPa)	$Z$ (m)	$T$ ( $^{\circ}\text{C}$ )	$q$ ( $\text{g kg}^{-1}$ )	RH (%)	$\theta$ (K)	$U$ ( $\text{m s}^{-1}$ )	WD ( $^{\circ}$ )
50	20541	-61.7	<i>0.004</i>	<i>2.2</i>	<i>497.7</i>	<i>13.0</i>	<i>262</i>
	20767	-61.8	<i>0.004</i>	<i>2.4</i>	<i>497.5</i>	<i>7.9</i>	<i>87</i>
	20879	-61.0	<i>0.004</i>	<i>2.0</i>	<i>499.2</i>	<i>10.5</i>	<i>86</i>
	<b>20646</b>	<b>-61.6</b>	<b><i>0.004</i></b>	<b><i>2.1</i></b>	<b><i>498.0</i></b>	<b><i>11.5</i></b>	<b><i>260</i></b>
100	16338	-67.7	<i>0.003</i>	<i>10.9</i>	<i>396.7</i>	<i>38.4</i>	<i>266</i>
	16606	-71.7	<i>0.004</i>	<i>22.3</i>	<i>388.9</i>	<i>17.8</i>	<i>274</i>
	16707	-72.3	<i>0.005</i>	<i>25.2</i>	<i>387.7</i>	<i>9.5</i>	<i>356</i>
	<b>16456</b>	<b>-69.3</b>	<b><i>0.004</i></b>	<b><i>16.0</i></b>	<b><i>393.6</i></b>	<b><i>29.1</i></b>	<b><i>268</i></b>
150	13860	-60.2	<i>0.01</i>	<i>11.0</i>	<i>366.2</i>	<i>54.6</i>	<i>266</i>
	14175	-63.4	<i>0.01</i>	<i>33.6</i>	<i>360.6</i>	<i>28.8</i>	<i>269</i>
	14287	-63.9	<i>0.02</i>	<i>46.6</i>	<i>359.7</i>	<i>15.3</i>	<i>286</i>
	<b>13998</b>	<b>-61.5</b>	<b><i>0.01</i></b>	<b><i>22.5</i></b>	<b><i>364.0</i></b>	<b><i>42.4</i></b>	<b><i>267</i></b>
200	12034	-52.5	<i>0.02</i>	<i>20.3</i>	<i>349.5</i>	<i>60.9</i>	<i>266</i>
	12364	-52.2	<i>0.08</i>	<i>51.8</i>	<i>349.9</i>	<i>30.9</i>	<i>264</i>
	12474	-51.0	<i>0.10</i>	<i>56.1</i>	<i>351.8</i>	<i>16.0</i>	<i>272</i>
	<b>12178</b>	<b>-52.2</b>	<b><i>0.05</i></b>	<b><i>33.8</i></b>	<b><i>350.0</i></b>	<b><i>46.8</i></b>	<b><i>266</i></b>
250	10570	-45.4	<i>0.07</i>	<i>28.3</i>	<i>338.5</i>	<i>57.1</i>	<i>265</i>
	10885	-41.2	<i>0.24</i>	<i>57.00</i>	<i>344.7</i>	<i>27.9</i>	<i>260</i>
	10984	-39.2	<i>0.27</i>	<i>52.1</i>	<i>347.6</i>	<i>14.2</i>	<i>261</i>
	<b>10706</b>	<b>-43.5</b>	<b><i>0.15</i></b>	<b><i>39.2</i></b>	<b><i>341.3</i></b>	<b><i>43.5</i></b>	<b><i>264</i></b>
300	9337	-38.8	<i>0.16</i>	<i>32.0</i>	<i>330.6</i>	<i>50.0</i>	<i>265</i>
	9621	-31.6	<i>0.51</i>	<i>54.2</i>	<i>340.7</i>	<i>24.7</i>	<i>257</i>
	9709	-29.5	<i>0.53</i>	<i>47.2</i>	<i>343.7</i>	<i>12.9</i>	<i>255</i>
	<b>9459</b>	<b>-35.7</b>	<b><i>0.31</i></b>	<b><i>39.8</i></b>	<b><i>334.9</i></b>	<b><i>38.2</i></b>	<b><i>264</i></b>
400	7312	-26.6	0.40	31.5	320.3	36.6	268
	7523	-17.0	1.33	51.4	332.8	20.0	256
	7593	-15.0	1.37	45.4	335.4	11.3	248
	<b>7404</b>	<b>-22.6</b>	<b>0.77</b>	<b>38.2</b>	<b>325.6</b>	<b>28.7</b>	<b>265</b>
500	5667	-16.2	0.68	28.8	313.2	26.9	271
	5813	-6.7	2.61	56.9	324.8	16.5	254
	5872	-5.0	2.77	52.9	326.9	10.7	245
	<b>5732</b>	<b>-12.3</b>	<b>1.45</b>	<b>39.0</b>	<b>318.0</b>	<b>21.9</b>	<b>267</b>
600	4281	-8.1	0.98	27.7	306.8	19.8	275
	4374	1.0	4.31	64.0	317.3	13.8	253
	4421	3.0	4.72	59.8	319.7	10.3	242
	<b>4324</b>	<b>-4.4</b>	<b>2.33</b>	<b>41.0</b>	<b>311.2</b>	<b>16.9</b>	<b>269</b>
700	3061	-1.8	1.37	28.9	300.4	14.1	282
	3111	7.4	6.29	69.4	310.7	11.5	248
	3148	10.1	7.27	66.1	313.6	10.7	236
	<b>3086</b>	<b>2.1</b>	<b>3.43</b>	<b>43.9</b>	<b>304.8</b>	<b>12.8</b>	<b>272</b>
850	1499	4.2	3.34	54.6	290.6	8.7	300
	1487	14.7	10.10	80.6	301.6	9.0	216
	1505	18.2	12.68	81.3	305.2	8.7	220
	<b>1497</b>	<b>8.8</b>	<b>6.37</b>	<b>64.8</b>	<b>295.4</b>	<b>8.8</b>	<b>276</b>
925	806	7.8	5.05	66.7	287.3	7.4	317
	765	18.0	11.81	82.6	297.7	7.1	167
	773	22.1	15.41	83.6	301.9	6.8	210
	<b>792</b>	<b>12.4</b>	<b>8.26</b>	<b>73.1</b>	<b>292.0</b>	<b>7.2</b>	<b>292</b>
1000	158	11.9	6.07	63.8	285.1	4.3	339
	98	21.9	12.91	76.3	295.1	3.5	59
	88	26.9	17.27	76.0	300.1	3.0	179
	<b>132</b>	<b>16.5</b>	<b>9.35</b>	<b>68.5</b>	<b>289.7</b>	<b>3.9</b>	<b>345</b>

Table 3: Surface and layer mean (850-500 hPa) sounding parameters for CNT (first row), MXD (second row), OCN (third row), and combined average (fourth row, bold).

$P$ (hPa)	$T$ ( $^{\circ}\text{C}$ )	$q$ ( $\text{g kg}^{-1}$ )	RH (%)	$\theta$ (K)	$U$ ( $\text{m s}^{-1}$ )	WD ( $^{\circ}$ )
1016	12.9	6.38	64.1	284.8	2.7	340
1008	22.9	13.41	75.5	295.3	2.7	37
1007	27.8	17.86	75.2	300.3	2.5	168
<b>995</b>	<b>16.8</b>	<b>9.67</b>	<b>67.6</b>	<b>286.5</b>	<b>2.7</b>	<b>345</b>
850-500 mean	-5.5	1.59	35.0	302.7	17.4	282
	4.1	5.82	67.8	313.6	12.7	243
	6.6	9.86	65.0	316.3	9.89	236
	<b>-1.4</b>	<b>3.39</b>	<b>47.2</b>	<b>307.3</b>	<b>15.1</b>	<b>269</b>



Table 4: Averages of stability, moisture indices, and rainfall for the CNT, MXD, OCN, and combined average for all sounding categories in the “concurrent” days subset. Rainfall-related values outside of brackets are calculated using all data, while values in brackets are calculated excluding rainfall values less than  $1 \text{ mm day}^{-1}$  or  $0.1 \text{ mm (10 min)}^{-1}$ .

	LCL (hPa)	CAPE ( $\text{J kg}^{-1}$ )	CIN ( $\text{J kg}^{-1}$ )	LI	PW (mm)	$\overline{R_d}$ ( $\text{mm day}^{-1}$ )	$\overline{R_{10}}$ [ $\text{mm (10 min)}^{-1}$ ]
CNT	891.0	5	-43	11.8	14.5	1.33 (1.48)	0.23 (0.26)
MXD	923.8	13	-110	3.8	43.1	14.79 (22.70)	1.95 (2.69)
OCN	924.7	581	-61	-1.9	52.8	13.00 (23.81)	2.69 (4.72)
<b>ALL</b>	<b>904.4</b>	<b>105</b>	<b>-65</b>	<b>7.7</b>	<b>27.5</b>	<b>8.42 (8.59)</b>	<b>1.45 (1.46)</b>